

## A wavelength-dependent visible and infrared spectrophotometric function for the Moon based on ROLO data

B. J. Buratti,<sup>1</sup> M. D. Hicks,<sup>1</sup> J. Nettles,<sup>2</sup> M. Staid,<sup>3</sup> C. M. Pieters,<sup>2</sup> J. Sunshine,<sup>4</sup> J. Boardman,<sup>5</sup> and T. C. Stone<sup>6</sup>

Received 30 August 2010; revised 26 October 2010; accepted 23 December 2010; published 5 April 2011.

[1] The USGS's Robotic Lunar Observatory (ROLO) dedicated ground-based lunar calibration project obtained photometric observations of the Moon over the spectral range attainable from Earth (0.347–2.39  $\mu\text{m}$ ) and over solar phase angles of 1.55°–97°. From these observations, we derived empirical lunar surface solar phase functions for both the highlands and maria that can be used for a wide range of applications. The functions can be used to correct for the effects of viewing geometry to produce lunar mosaics, spectra, and quick-look products for future lunar missions and ground-based observations. Our methodology can be used for a wide range of objects for which multiply scattered radiation is not significant, including all but the very brightest asteroids and moons.

**Citation:** Buratti, B. J., M. D. Hicks, J. Nettles, M. Staid, C. M. Pieters, J. Sunshine, J. Boardman, and T. C. Stone (2011), A wavelength-dependent visible and infrared spectrophotometric function for the Moon based on ROLO data, *J. Geophys. Res.*, 116, E00G03, doi:10.1029/2010JE003724.

### 1. Introduction and Scope

[2] Much of the variation in specific intensity and spectral albedo on the Moon, or any other planetary body, is not intrinsic but rather due to changing radiance viewing geometry. A number of studies have provided evidence for the significant influence of viewing geometry on spectral reflectance, including those of *Gradie and Veverka* [1982], *Pieters et al.* [1991] and *Domingue and Vilas* [2007]. In order to produce photometrically correct mosaics and to detect and map subtle spectral features of minerals and volatiles on the lunar surface, such as iron- and titanium-bearing minerals and water ice, a quantitative model describing the directional properties of reflected solar radiation must be developed as a function of wavelength. With the advancement of lunar studies over the past decade, specifically mapping of surface components that hold scientific value for future study and exploration of the Moon, it is important to develop such a model for use with a wide range of lunar cameras and spectrometers.

[3] NASA's Moon Mineralogy Mapper (M<sup>3</sup>), an imaging spectrometer that was included as part of the scientific payload on Indian Space Agency's Chandrayaan-1 spacecraft

and gathered data throughout two mapping periods in 2008–2009 [*Pieters et al.*, 2007, 2009], provided a motivation to develop a spectrophotometric model for the visible and near infrared. The database used for the model was produced from the USGS's Robotic Lunar Observatory (ROLO) dedicated ground-based lunar calibration project [*Kieffer and Wildey*, 1996; *Kieffer and Stone*, 2005]. One purpose of this investigation was to develop a model that can be used by a wide variety of lunar investigations in the visible and near-IR. Our general, relatively simple model expresses the variations on the surface of the Moon due to changes in the solar phase function, and it is based entirely on measurements from ROLO. The alternative, to use derived radiative transfer model parameters such as the single scattering albedo, the single scattering phase function, opposition surge and roughness parameters [*Chandrasekhar*, 1960; *Hapke*, 1981, 1984, 1986, 1990], all of which vary with position on the Moon, entails complicated, nonunique model fits and assumptions that are of limited use in constructing data sets from spacecraft observations. These data sets include maps of minerals and volatiles, multispectral mosaics corrected for the effects of viewing geometry (phase angle, incident angle, and emission angle), and extracted spectra.

### 2. Data Analysis

#### 2.1. ROLO Data

[4] The need for a well-characterized calibration target for space-based and ground-based remote-sensing studies was realized decades ago. A dedicated program to gather photometric data for the Moon over the spectral range attainable from Earth (0.347–2.39  $\mu\text{m}$ ) and over solar phase angles of 1.55°–97°, was initiated by Hugh Kieffer and his colleagues

<sup>1</sup>Jet Propulsion Laboratory, California Institute of Technology, Pasadena, California, USA.

<sup>2</sup>Department of Geological Sciences, Brown University, Providence, Rhode Island, USA.

<sup>3</sup>Planetary Science Institute, Tucson, Arizona, USA.

<sup>4</sup>Department of Astronomy, University of Maryland, College Park, Maryland, USA.

<sup>5</sup>Analytical Imaging and Geophysics, Boulder, Colorado, USA.

<sup>6</sup>U.S. Geological Survey, Flagstaff, Arizona, USA.

**Table 1.** ROLO Chip Locations<sup>a</sup>

Chip Number	Name	Selenographic Location	
		Latitude (°)	Longitude (°)
0	Mare Serenitatus	19.06	20.47
1	East edge	-5.81	69.80
2	North edge	70.46	-16.27
3	South edge	-71.06	-28.64
4	West edge	-2.62	-73.88
5	Aristarchus 3	23.30	-47.35
6	Aristarchus 7	23.30	-47.35
7	Copernicus	9.48	-20.11
8	Tycho	-43.50	-11.06
9	Highlands	-17.21	20.01
10	Tycho ray	-37.09	-16.88

<sup>a</sup>Adapted from *Kieffer and Stone* [2005].

at the USGS Astrogeology Center under NASA sponsorship [*Kieffer and Wildey*, 1996]. Extensive measurements have been published [*Kieffer and Stone*, 2005], and calibrated telescopic images and additional data provided by the USGS have been used for this study. In particular, 11 lunar regions that were the subject of focused analysis by *Kieffer and Stone* [2005] provided extensive radiometric measurements and phase information. These areas (“chips”) are listed in Table 1. The chips include small areas of about  $20 \times 20$  km that are represented by  $3 \times 3$  pixel squares in a modified Lambert azimuthal equal area projection of the ROLO images.

## 2.2. The Photometric Model

[5] We obtained 36,000 photometric data points from the ROLO observations for each of the 11 reference regions defined by *Kieffer and Stone* [2005]. Exoatmospheric radiance data was further calibrated to units of reflectance through normalization over a solar irradiance model. Observations from the waxing phases were selected and corrected for “limb-darkening” (changes in specific intensity due to changes in the incidence and emission angle) to derive a

surface solar phase function using the following equation [*Seeliger*, 1884; *Chandrasekhar*, 1960]:

$$I/F = f(\alpha)[\mu_o/(\mu + \mu_o)] \quad (1)$$

where  $\mu_o$  is the cosine of the incident angle,  $\mu$  is the cosine of the emission angle, and  $f(\alpha)$  is the surface solar phase function. This lunar scattering law (given by the  $\mu_o/(\mu + \mu_o)$  term), which has been known since the nineteenth century and follows from the equation of radiative transfer, is often called the Lommel-Seeliger function after two early users of the model for the lunar surface. The solar phase function includes the physical effects of macroscopic roughness; the single particle phase function describing the directional scattering properties of individual particles; the single scattering albedo; and the opposition effect. This latter effect is the nonlinear increase in brightness that nearly all airless bodies exhibit as their surfaces become fully illuminated to an observer [*Irvine*, 1966; *Hapke*, 1986]. The surge is due to both the rapid disappearance of mutual shadows cast among regolith particles and to coherent backscatter [*Hapke*, 1990]. The Moon is known to exhibit a strong opposition surge due to both effects and the surge has been modeled from Clementine data based on physical parameters [*Buratti et al.*, 1996; *Hillier et al.*, 1999]. In this empirical approach designed to provide a simple photometric function for use with spacecraft observations, we concatenate all the physical parameters into the single function  $f(\alpha)$ . Examples of the derived solar phase functions  $f(\alpha)$  over the spectral range of the ROLO measurements for both mare and highlands are shown in Figure 1. The wavelength dependence for the solar phase function at  $10^\circ$  intervals is shown in Figure 2.

[6] We used the waxing phase for our fits because these observations were less noisy and fit the observations better. Also, the fits to the waning phases exhibited more discontinuities due to filter gaps in the ROLO data and discontinuities near absorption band positions. The jags remaining in the waxing fits have been smoothed over in our final photometric model. The causes of the differences

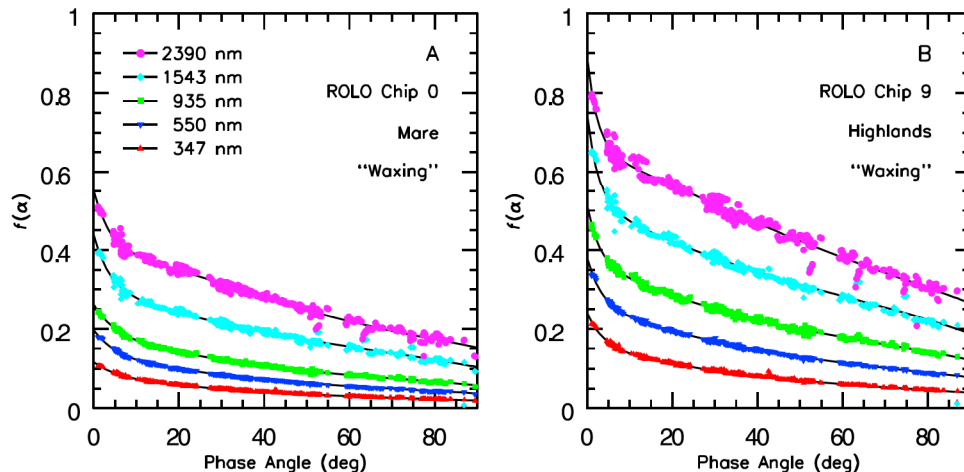


**Figure 1.** (a) The solar phase curve of Mare Serenitatis, extracted from the ROLO data at five wavelengths spanning the spectral range of the instrument. (b) The phase curve for the lunar highlands. The dark line is the functional fit to each curve (equation (2)). The color codes are the same for Figures 1a and 1b.

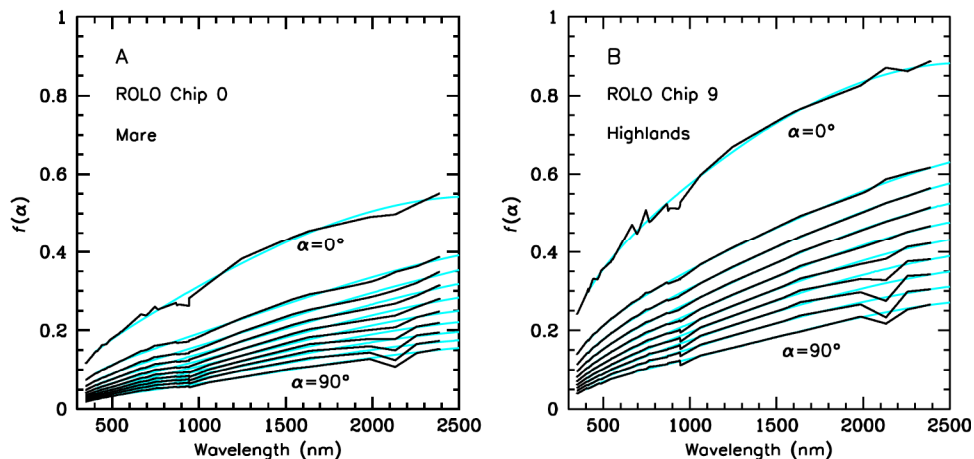


**Figure 2.** The solar phase function of the same regions, as a function of wavelength at  $10^\circ$  intervals. The unsmoothed (black) line is the fit from the ROLO data, while the blue line is smoothed across the filter boundaries.

between the waxing and waning phases are discussed more fully in section 4 and in the work of *Goguen et al.* [2010].

### 2.3. Methodology

[7] The steps to create a readily useable lunar photometric function based on ROLO data are as follows:

[8] 1. Solar phase functions ( $f(\lambda, \alpha)$ ) were extracted for each of the 11 sites employing equation (1).

[9] 2. Chip 0 was chosen as typical for mare regions and chip 9 was chosen as typical for the lunar highlands.

[10] 3. The surface phase functions were then fit to a fourth-order polynomial plus an exponential term. Interpolations were done to produce a model at one nanometer resolution.

[11] 4. A file giving the solar phase corrections at one degree in  $\alpha$  and one nanometer in spectral granularity was produced. The range in solar phase angle is  $0-90^\circ$  and the range in wavelength is  $0.347-2.39 \mu\text{m}$  (from ROLO). The fits to the polynomial were also extrapolated to a wavelength of  $3.0 \mu\text{m}$  to cover the wavelength range of the  $M^3$  instrument. This file can be used as a preliminary solar phase function for a wide variety of lunar missions that have visible and infrared cameras. Tables 2 and 3 give the values of equation (2) for typical highlands and maria regions.

[12] Modeling the lunar solar phase function to correct  $M^3$  spectral image cubes and other potential lunar data sets entails fitting the extracted solar phase functions (Step 1 above) to the 11 ROLO focus regions at each of the 32 wavelengths of the ROLO filters. We found that a fourth-order polynomial, with an extra exponential term to model the opposition surge region fit well:

$$f(\alpha, \lambda) = C_0 e^{-C\alpha} + A_0 + A_1 \alpha + A_2 \alpha^2 + A_3 \alpha^3 + A_4 \alpha^4 \quad (2)$$

The fits for chips that well represent both lunar maria and the highlands are listed in Tables 2 and 3. For the mare, we used ROLO data from chip 0 (Mare Serenitatis) and for the highlands we used data from chip 9 (Highlands). These solar phase functions can be employed to correct the reflectance of the Moon for the effects of viewing geometry.

[13] These fits to the visible and near-IR surface photometric function of the Moon can be used for a wide variety

of calibration purposes. They can be used to approximate a photometric function for any region on the Moon by coadding appropriate fractions of photometric functions for the highlands and maria.

### 2.4. Validation With Apollo 16 Data

[14] Of all celestial bodies, the Moon has the advantage that ground truth has been obtained for it. One example of the use of the ROLO solar phase functions is a photometric correction to reference the lunar surface to samples from the Apollo 16 landing site. Extensive calibrations of the Apollo 16 landing site samples have been performed at Brown University's RELAB facility [*Pieters, 1983, 1999*]. Thus, it is desirable to obtain a reference photometric function for this site. Unfortunately, the Apollo landing site was not one of the 11 ROLO sites chosen for focused study. However, a good approximation to the photometric behavior of the site can be obtained by coadding fractions of highland and maria; the correct partition between highland and maria is obtained when the spectrum of the coadded  $f(\alpha)$  matches the ROLO spectrum of the Apollo landing site. Figure 3 shows the result of this process for the Apollo 16 region; these results were created by mixing the highland and mare solar phase functions in a combination that gave consistency with the measured spectrum and albedo of the landing site at a solar phase angle of  $30^\circ$ , the geometry of the RELAB measurements. For this specific case, the highlands were 84% of the solar phase function and resulting spectrum, while the maria were 16%. (The actual fraction of highlands was 1.19 and the fraction of maria was 0.19. The numbers do not sum to unity because an adjustment had to be made for the higher albedo of the Apollo 16 region). The Apollo 16 landing site was in the highlands southwest of Mare Tranquillitatis, but the specific location was in the Cayley Plains, which could have some characteristics of the lunar maria. Thus, a photometric function that is 16% maria makes sense.

[15] The specific photometric correction used to reference observations to that of the Apollo site normalized to  $30^\circ$  is given by:

$$f(\text{Apollo16}, 30^\circ, \lambda) / f(\text{Apollo16}, \alpha, \lambda) \quad (3)$$

**Table 3.** ROLO-Derived Irradiance Model Coefficients (Equation (2)): Highlands

$\lambda_{\text{eff}}$ (nm)	Spectral Channel	$C_0$ ( $\times 10^{-2}$ )	$C_1$	$A_0$	$A_1$ ( $\times 10^{-2}$ )	$A_2$ ( $\times 10^{-4}$ )	$A_3$ ( $\times 10^{-6}$ )	$A_4$ ( $\times 10^{-8}$ )
0347	V	0.2760	0.0795	0.1610	-0.3010	0.3125	-0.1598	0.0184
0353	V	0.2650	0.0816	0.1626	-0.2917	0.2820	-0.1256	0.0043
0405	V	0.2880	0.0956	0.1990	-0.3482	0.3312	-0.1434	0.0051
0413	V	0.3080	0.0999	0.2058	-0.3912	0.4767	-0.3570	0.1097
0415	V	0.2900	0.0972	0.2012	-0.3599	0.3804	-0.2157	0.0366
0442	V	0.3350	0.1070	0.2245	-0.4351	0.5688	-0.4579	0.1487
0467	V	0.2820	0.1039	0.2257	-0.3789	0.3725	-0.1914	0.0248
0476	V	0.3000	0.1027	0.2339	-0.4071	0.4301	-0.2460	0.0432
0488	V	0.3200	0.1105	0.2416	-0.4341	0.5152	-0.3818	0.1136
0545	V	0.2880	0.1167	0.2582	-0.3779	0.2358	0.0366	-0.0907
0550	V	0.2980	0.1161	0.2633	-0.4059	0.3387	-0.1143	-0.0173
0555	V	0.2940	0.1189	0.2616	-0.3829	0.2472	0.0253	-0.0884
0667	V	0.4190	0.1551	0.3160	-0.5360	0.6431	-0.4926	0.1473
0695	V	0.3260	0.1328	0.3147	-0.4613	0.3850	-0.1449	-0.0122
0706	V	0.3300	0.1400	0.3164	-0.4474	0.3344	-0.0842	-0.0367
0747	V	0.4710	0.1596	0.3492	-0.6244	0.8679	-0.7811	0.2762
0766	V	0.3630	0.1364	0.3418	-0.5428	0.6177	-0.4369	0.1107
0777	V	0.3620	0.1383	0.3429	-0.5298	0.5634	-0.3686	0.0829
0868	V	0.3860	0.1546	0.3703	-0.5714	0.6415	-0.4968	0.1533
0875	V	0.3460	0.1481	0.3587	-0.4774	0.3325	-0.0606	-0.0563
0885	V	0.3600	0.1513	0.3623	-0.4992	0.4060	-0.1647	-0.0056
0935	V	0.3540	0.1417	0.3707	-0.4937	0.3315	0.0003	-0.1109
0944	V	0.3920	0.1403	0.3788	-0.5366	0.4505	-0.1328	-0.0610
0944	I	0.2480	0.1989	0.3293	-0.0446	-1.1729	1.9249	-0.9619
1062	I	0.3200	0.1904	0.4073	-0.4939	0.2562	0.1572	-0.2263
1247	I	0.3350	0.2211	0.4479	-0.4533	0.0292	0.4511	-0.3605
1543	I	0.3790	0.2222	0.5221	-0.5690	0.3279	0.0295	-0.1661
1638	I	0.3470	0.2292	0.5368	-0.5240	0.1804	0.2442	-0.2928
1985	I	0.3150	0.2588	0.5667	-0.1977	-0.9354	1.3914	-0.6249
2132	I	0.4940	0.1997	0.6712	-1.0504	2.3087	-3.7733	2.0916
2256	I	0.3960	0.2018	0.6603	-0.6550	0.3860	-0.0610	-0.1306
2390	I	0.4110	0.2311	0.6568	-0.4008	-0.4371	0.8108	-0.4070

**Table 2.** ROLO-Derived Irradiance Model Coefficients (Equation (2)): Mare

$\lambda_{\text{eff}}$ (nm)	Spectral Channel	$C_0$ ( $\times 10^{-2}$ )	$C_1$	$A_0$	$A_1$ ( $\times 10^{-2}$ )	$A_2$ ( $\times 10^{-4}$ )	$A_3$ ( $\times 10^{-6}$ )	$A_4$ ( $\times 10^{-8}$ )
0347	V	0.1830	0.0359	0.0807	-0.1371	0.1016	-0.0092	-0.0213
0353	V	0.1670	0.0398	0.0786	-0.1141	0.0402	0.0577	-0.0478
0405	V	0.2000	0.0467	0.0995	-0.1625	0.1039	0.0191	-0.0400
0413	V	0.1900	0.0486	0.0994	-0.1631	0.1199	-0.0155	-0.0198
0415	V	0.1850	0.0490	0.0984	-0.1535	0.0919	0.0211	-0.0383
0442	V	0.2200	0.0503	0.1126	-0.2091	0.2176	-0.1114	0.0138
0467	V	0.1740	0.0580	0.1072	-0.1407	0.0239	0.1109	-0.0774
0476	V	0.1900	0.0544	0.1155	-0.1808	0.1167	0.0143	-0.0406
0488	V	0.2140	0.0554	0.1209	-0.2088	0.1845	-0.0581	-0.0126
0545	V	0.1820	0.0697	0.1242	-0.1299	-0.1056	0.3244	-0.1856
0550	V	0.2020	0.0653	0.1322	-0.1891	0.0786	0.0873	-0.0794
0555	V	0.1940	0.0668	0.1301	-0.1684	0.0123	0.1741	-0.1194
0667	V	0.2420	0.0751	0.1661	-0.2718	0.2389	-0.0828	-0.0119
0695	V	0.2060	0.0763	0.1615	-0.2146	0.0638	0.1344	-0.1070
0706	V	0.1950	0.0843	0.1573	-0.1654	-0.0769	0.2973	-0.1743
0747	V	0.2510	0.0754	0.1849	-0.3226	0.3544	-0.2184	0.0453
0766	V	0.2000	0.0777	0.1751	-0.2456	0.1532	0.0114	-0.0506
0777	V	0.2020	0.0812	0.1741	-0.2225	0.0618	0.1383	-0.1095
0868	V	0.2140	0.0863	0.1838	-0.2465	0.1148	0.0714	-0.0772
0875	V	0.2030	0.0866	0.1774	-0.2027	-0.0152	0.2359	-0.1511
0885	V	0.2100	0.0867	0.1797	-0.2168	0.0207	0.1958	-0.1349
0935	V	0.1830	0.0888	0.1741	-0.1579	-0.1557	0.4259	-0.2426
0944	V	0.1860	0.0831	0.1794	-0.1943	-0.0553	0.3151	-0.2009
0944	I	0.1700	0.1352	0.1467	0.1190	-1.0138	1.4590	-0.6728
1062	I	0.2230	0.1139	0.2078	-0.2390	0.0309	0.2173	-0.1646
1247	I	0.2510	0.1416	0.2411	-0.1913	-0.3161	0.7924	-0.4712
1543	I	0.2650	0.1381	0.3013	-0.3251	0.0771	0.2042	-0.1774
1638	I	0.2500	0.1459	0.3094	-0.2958	-0.0183	0.3414	-0.2584
1985	I	0.2060	0.1883	0.3024	0.0667	-1.1542	1.5768	-0.6852
2132	I	0.2650	0.1048	0.3928	-0.5994	0.9454	-1.3068	0.6721
2256	I	0.2830	0.1319	0.3925	-0.3849	0.0953	0.1415	-0.1275
2390	I	0.2590	0.1606	0.3909	-0.0659	-0.9753	1.3711	-0.5908

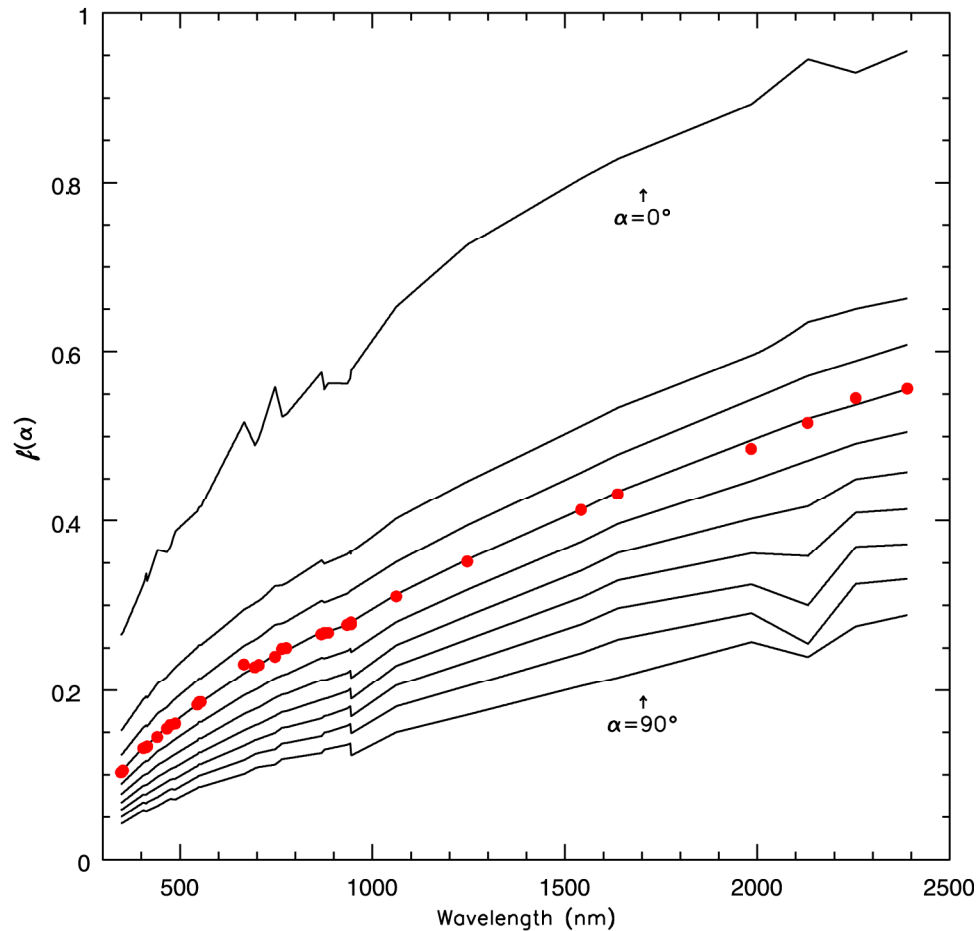


**Figure 3.** The solar phase function of the Apollo 16 landing site, shown as a function of wavelength at  $10^\circ$  intervals. The fits are based on coadding fractions of the mare and highland ROLO sites. The Apollo 16 spectrum from RELAB data [Pieters, 1983, 1999] is shown in red. This spectrum is represented by 84% highlands and 16% maria.

Detailed spectroscopic analyses of the Moon require a smooth file of the solar phase correction factor at  $\sim$ one nanometer increments in wavelength and one degree increments in solar phase angle. These corrections are illustrated graphically in Figure 4 for equation (3). These data have been smoothed and extrapolated with the fit polynomial to  $3.0 \mu\text{m}$ , the upper limit to the wavelength range of  $M^3$ . This exercise illustrates that the photometric function of any region on the Moon, with the exception of the bright ray craters, can be constructed from the appropriate partitioning of the solar phase functions of highlands and maria.

### 3. Application to $M^3$ Data

[16]  $M^3$  observations from the initial data-taking phase (OP1) were extracted and converted to solar phase functions by multiplying  $I/F$  values by  $(\mu + \mu_0)/\mu_0$ , which is the inverse of the Lommel-Seeliger term. The resulting solar phase function  $f(\alpha)$  (Figure 5) shows good agreement with the ROLO solar phase function. There is a fair amount of scatter in the  $M^3$  data due to roughness and albedo variations, but there is consistency in overall shape between

the two phase functions. Figures 6a and 6b show an early  $M^3$  mosaic with the photometric effects corrected with the ROLO photometric model for highlands. The derivation of a solar phase function based on the  $M^3$  data is the subject of Hicks *et al.* [2011].

### 4. Discussion and Conclusions

[17] From ROLO data we have produced an empirical, wavelength-dependent solar surface phase function for two end-members of the lunar terrain: highlands and maria. These results can be used for quick-look, outreach, and initial mosaics produced by cameras and imaging spectrometers on lunar missions. More detailed models based on actual data acquired by these instruments will of course be used for more advanced scientific analysis such as identification of subtle spectral bands of minerals and volatiles [Hicks *et al.*, 2011]. An assessment of the importance of thermal radiation (mainly for wavelengths larger than  $\sim 2.5 \mu\text{m}$ ) was not done on these data sets. Note that our fits are entirely empirical: no attempt is made to derive photometric parameters for roughness, single particle phase functions, single scattering albedo, and opposition surge

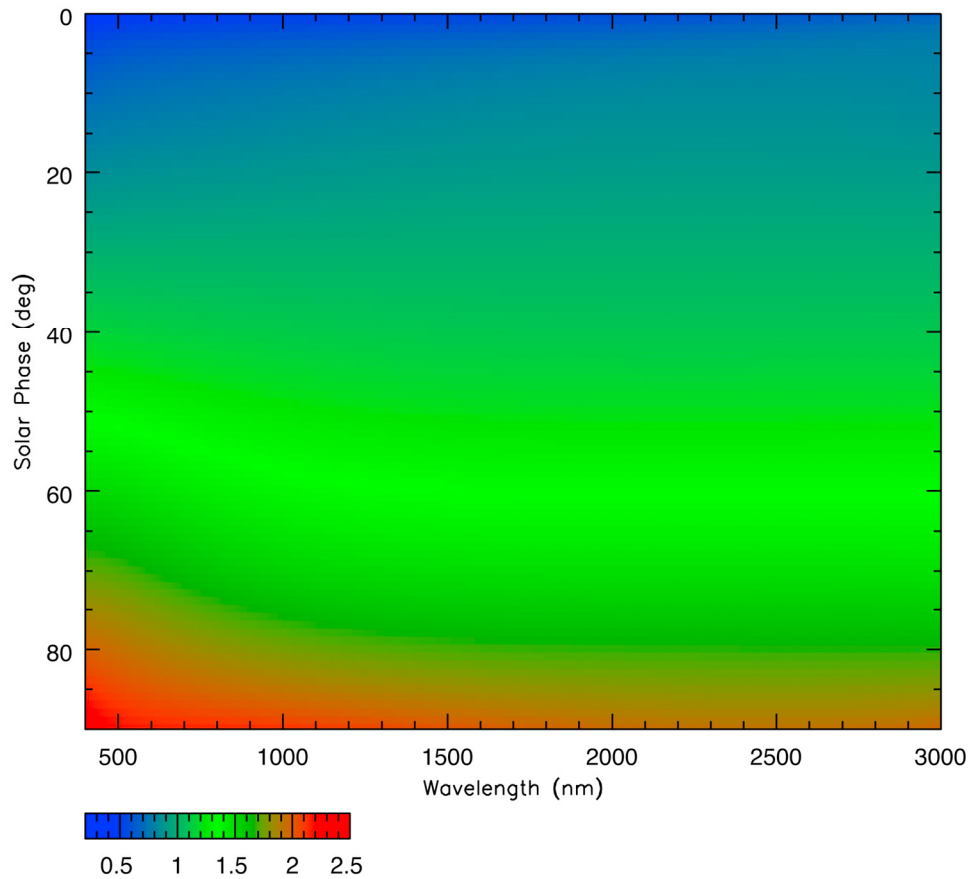


**Figure 4.** An initial smoothed relative solar phase correction factor based on the above photometric model for Apollo 16. This model would correct observations with the solar phase behavior of the Apollo 16 landing site to the geometry of the RELAB spectra, which were obtained at a 30 degrees “solar” phase angle and an emission angle of 30°. Color indicates the intensity of the correction. Because the fitted solar phase functions have been normalized to a standard viewing geometry of 30° solar phase, the values of these correction factors are all unity at 30°.

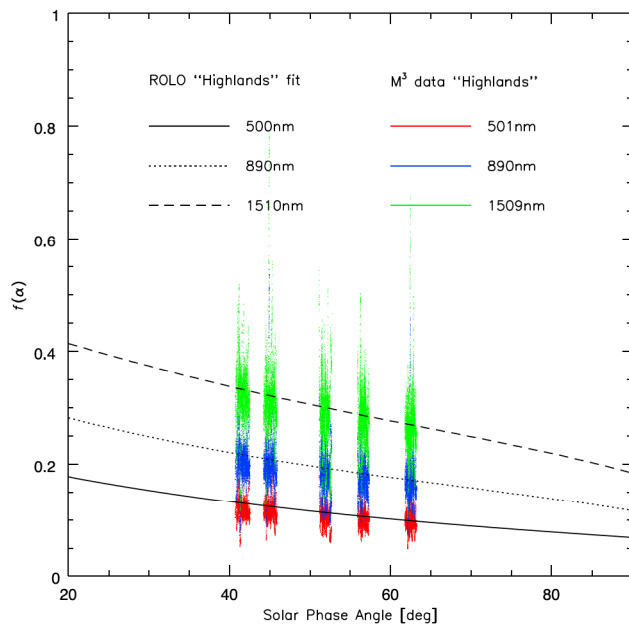
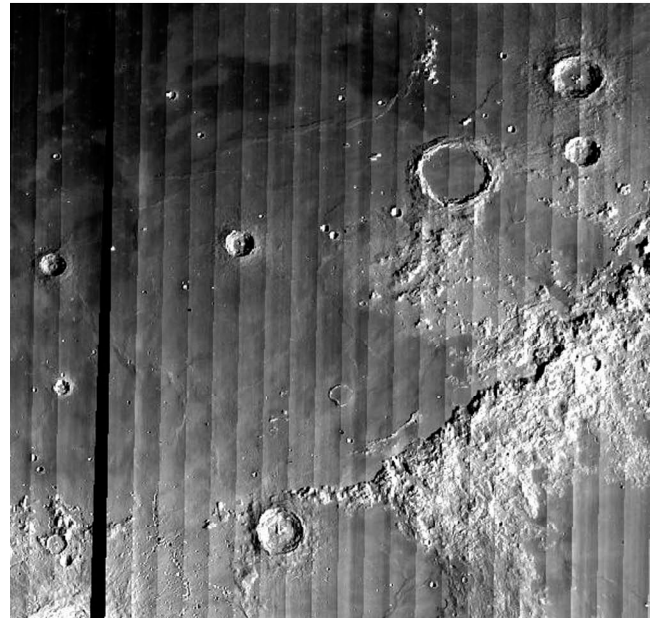


**Figure 5.** The first  $M^3$  lunar photometric function compared with the ROLO model, showing good agreement. The  $M^3$  observations were extracted from within a  $5^\circ \times 5^\circ$  square box centered on a latitude of  $-17.21^\circ$  and a longitude of  $15.01^\circ$ , which is near ROLO chip 9 (early data were not obtained at the exact location of chip 9). The  $M^3$  observations were averaged into 5 equal segments along the cross track direction. The data depicted have been corrected for the Lommel-Seeliger factor.

parameters [see, e.g., Hapke, 1981, 1984, 1986; Buratti, 1985], since these parameters are often impossible to uniquely fit [Helfenstein *et al.*, 1988] and may not accurately portray physical truth [Shepard and Helfenstein, 2007]. Appropriate fractions of the lunar highlands and maria functions can be coadded to fit any lunar terrain, except bright ray craters. Finally, our simple methodology can be applied to any airless celestial body for which multiple scattering is not important, including all but the most reflective asteroids, and moons with albedos less than  $\sim 0.6$  [Buratti, 1984].

[18] It is also important to note that the waxing and waning phases of the Moon exhibit different photometric functions in the ROLO data. Although the principle of reciprocity requires that the interchange of the incident and emission angle results in identical fits to a photometric function, the specific case of the Moon is complicated by lunar macroscopic roughness [Goguen *et al.*, 2010]. For the waning phases of the Moon, large emission angles are in regions where the effects of shadowing by craters, mountains, and clumps of particles are greatest. In addition, these features alter the local viewing geometry from that expected for a simple sphere. (The well-known, smaller difference in the waxing and waning disk-integrated solar phase curves is due to another cause: the enhanced placement of low-albedo maria regions on the waning Moon). As stated in section 2, we used the waxing phase for our fits because these observations were less noisy and fit the observations better.



a.



b.

**Figure 6.** An early  $M^3$  image corrected with the ROLO photometric model for the highlands. (a) No photometric correction. (b) With the “Lommel-Seeliger” correction applied and the solar phase function described in Table 3.

[19] **Acknowledgments.** This research was carried out at the Jet Propulsion Laboratory, California Institute of Technology, under contract to the National Aeronautics and Space Administration. We thank Deborah Domingue for a detailed review.

## References

- Buratti, B. J. (1984), Voyager disk resolved photometry of the Saturnian satellites, *Icarus*, *59*, 392–405, doi:10.1016/0019-1035(84)90109-X.
- Buratti, B. J. (1985), Application of a radiative transfer model to bright icy satellites, *Icarus*, *61*, 208–217.
- Buratti, B. J., J. Hillier, and M. Wang (1996), The lunar opposition surge: Observations by Clementine, *Icarus*, *124*, 490–499, doi:10.1006/icar.1996.0225.
- Chandrasekhar, S. (1960), *Radiative Transfer*, Dover, New York.
- Domingue, D., and F. Vilas (2007), Local topographic effects on photometry and reflectance spectra of planetary surfaces: An example based on lunar photometry, *Meteorit. Planet. Sci.*, *42*, 1801–1816, doi:10.1111/j.1945-5100.2007.tb00539.x.
- Goguen, J. D., T. C. Stone, H. H. Kieffer, and B. J. Buratti (2010), A new look at photometry of the Moon, *Icarus*, *208*, 548–557, doi:10.1016/j.icarus.2010.03.025.
- Gradie, J., and J. Veverka (1982), When are spectral reflectance curves comparable?, *Icarus*, *49*, 109–119, doi:10.1016/0019-1035(82)90060-4.
- Hapke, B. (1981), Bidirectional reflectance spectroscopy: 1. Theory, *J. Geophys. Res.*, *86*, 3039–3054, doi:10.1029/JB086iB04p03039.
- Hapke, B. (1984), Bidirectional reflectance spectroscopy: 3. Correction for macroscopic roughness, *Icarus*, *59*, 41–59, doi:10.1016/0019-1035(84)90054-X.
- Hapke, B. (1986), Bidirectional reflectance spectroscopy: 4. The extinction coefficient and the opposition effect, *Icarus*, *67*, 264–280, doi:10.1016/0019-1035(86)90108-9.
- Hapke, B. (1990), Coherent backscatter and the radar characteristics of outer planet satellites, *Icarus*, *88*, 407–417, doi:10.1016/0019-1035(90)90091-M.
- Helfenstein, P., J. Veverka, and P. C. Thomas (1988), Uranus satellites: Hapke parameters from Voyager disk integrated photometry, *Icarus*, *74*, 231–239, doi:10.1016/0019-1035(88)90039-5.
- Hicks, M. D., et al. (2011), A photometric function for analysis of lunar images in the visual and infrared based on Moon Mineralogy Mapper observations, *J. Geophys. Res.*, doi:10.1029/2010JE003733, in press.
- Hillier, J. K., B. J. Buratti, and K. Hill (1999), Multispectral photometry of the Moon and absolute calibration of the Clementine UV/VIS camera, *Icarus*, *141*, 205–225, doi:10.1006/icar.1999.6184.
- Irvine, W. M. (1966), The shadowing effect in diffuse radiation, *J. Geophys. Res.*, *71*, 2931–2937.
- Kieffer, H. H., and T. S. Stone (2005), The spectral irradiance of the Moon, *Astron. J.*, *129*, 2887–2901, doi:10.1086/430185.
- Kieffer, H. H., and R. L. Wildey (1996), Establishing the Moon as a spectral Radiance standard, *J. Atmos. Oceanic Technol.*, *13*, 360–375, doi:10.1175/1520-0426(1996)013<0360:ETMAAS>2.0.CO;2.
- Pieters, C. (1983), Strength of mineral absorption features in the transmitted component of near-infrared reflected light: First results from RELAB, *J. Geophys. Res.*, *88*, 9534–9544, doi:10.1029/JB088iB11p09534.
- Pieters, C. M. (1999), The Moon as a calibration standard enabled by lunar samples, abstract 8025 presented at New Views of the Moon II: Understanding the Moon through the Integration of Diverse Datasets, U.S. Geological Survey, 22–24 Sept. (Available at [http://www.planetary.brown.edu/relabdocs/Apollo16\\_62231.html](http://www.planetary.brown.edu/relabdocs/Apollo16_62231.html))
- Pieters, C. M., S. Pratt, H. Hoffman, and P. Helfenstein (1991), Bidirectional spectroscopy of returned lunar soils: Detailed “ground truth” for planetary remote sensors, *Proc. Lunar Planet. Sci. Conf.*, *22*, 1069–1070.
- Pieters, C. M., et al. (2007), M<sup>3</sup> on Chandrayaan-1: Strategy for mineral assessment of the Moon, *Lunar Planet. Sci.*, *XXXVIII*, Abstract 1295.
- Pieters, C. M., et al. (2009), Character and spatial distribution of OH/H<sub>2</sub>O on the surface of the Moon seen by M<sup>3</sup> on Chandrayaan-1, *Science*, *326*, 568–572, doi:10.1126/science.1178658.
- Seeliger, H. (1884), Zur Photometrie des Saturnrings, *Astron. Nachr.*, *109*, 305–314, doi:10.1002/asna.18841092002.
- Shepard, M. K., and P. Helfenstein (2007), A test of the Hapke photometric model, *J. Geophys. Res.*, *112*, E03001, doi:10.1029/2005JE002625.
- J. Boardman, Analytical Imaging and Geophysics, Boulder, CO 80303, USA.
- B. J. Buratti and M. D. Hicks, Jet Propulsion Laboratory, California Institute of Technology, 4800 Oak Grove Dr., M. S. 183-401, Pasadena, CA 91109, USA. ([bonnie.j.buratti@jpl.nasa.gov](mailto:bonnie.j.buratti@jpl.nasa.gov))
- J. Nettles and C. M. Pieters, Department of Geological Sciences, Brown University, Providence, RI 02912, USA.
- M. Staid, Planetary Science Institute, Tucson, AZ 85719, USA.
- T. C. Stone, USGS, Flagstaff, AZ 86001, USA.
- J. Sunshine, Department of Astronomy, University of Maryland, College Park, MD 20742, USA.